AIAA SciTech Forum
11–15 & 19–21 January 2021, VIRTUAL EVENT
AIAA Scitech 2021 Forum

10.2514/6.2021-1551

High-Fidelity CFD Workshop 2022: Mesh Motion

Per-Olof Persson*
University of California, Berkeley, Berkeley, CA, United States
Lawrence Berkeley National Laboratory, Berkeley, Berkeley, CA, United States

Krzysztof Fidkowski†
University of Michigan, Ann Arbor, MI, USA

Nathan A. Wukie‡
Air Force Research Laboratory, Wright-Patterson AFB, United States

A mesh motion test case has been part of the High-Fidelity (previously High-Order) CFD Workshop since its inception in 2012. The number of groups participating has been small, and most submissions have used an Arbitrary Lagrangian Eulerian formulation, although this is not required. The initial cases involved the interaction of moving airfoils and cylinders in viscous flow. While reasonable agreement was obtained, the cases were too complex for exact data matching. Over the subsequent workshops, definitions of the test cases were made more precise, and agreement improved. However, even in the most recent workshop, a persistent difference in results could not be explained by lack of convergence in space or time, as each group performed refinement studies. This has motivated a reformulation of the mesh motion test case, with emphasis on verification: simpler geometries, smoother motions, and smaller problems that allow for more detailed convergence studies. This paper describes the resulting suite of cases and shows preliminary data from the case organizers.

Nomenclature

$\boldsymbol{u}$	Fluid state vector
ρ	Density
v_i	i-th component of velocity
E	Stagnation/total energy
M	Mach number
γ	Ratio of specific heats
W	Work
I	Impulse
$\vec{F}$	Force vector
$\vec{\tau}$	Torque vector
$\vec{v}_0$	Pivot velocity
$\vec{\omega}_0$	Angular velocity about pivot
m	Fluid mass
e_m	Mass conservation error
h	Height

*Professor, Department of Mathematics, University of California, Berkeley
Faculty Scientist, Mathematics Group, Lawrence Berkeley National Laboratory, AIAA Senior Member.
†Associate Professor, Department of Aerospace Engineering, University of Michigan, AIAA Senior Member.
‡Research Engineer, Multidisciplinary Science & Technology Center, Air Force Research Laboratory, AIAA Senior Member.

θ Angular position
c Airfoil chord
α Prescribed-motion function
β Prescribed-rotation function
A_i Amplitudes of motion
WU Work Unit

I. Introduction

This is an invited paper for the SciTech 2021 special session: High-Fidelity CFD Preworkshop. Fluid problems with moving or deforming domains are found in many important aerospace applications. Fluid-structure interaction, turbomachinery, store separation, and rotor-craft simulations are just a small subset of problems where the prediction of fluid phenomena on moving domains is very important. As a part of the High-Fidelity CFD Workshop, previously known as the High-Order Workshop [1], we seek to provide a Mesh Motion suite of problems for the purpose of supporting code verification activity as well as resolving outstanding challenges (for example, where agreement between datasets has not yet been established).

The Mesh Motion test suite is aimed at testing the accuracy and performance of high-order flow solvers for problems with moving and deforming domains. Two sets of test cases are considered: a cylinder and an airfoil. The cylinder cases involve a smaller domain and are intended to serve as verification simulations. The NACA 0012 problem is larger and has exhibited spread in the results in previous workshops. For both geometries, multiple motions are defined, and for the cylinder case, simulations at multiple Reynolds numbers are requested. The sections below describe the setup of each case. The outputs are defined similarly for both geometries, and a uniform data submission format is outlined in the requirements section.

II. Flow in a cylinder

A. Geometry

The reference geometry for this problem is a perfect cylinder for which several types of motion are prescribed. The center of motion coincides with the geometric center of the cylinder, and the fluid domain of interest is the cylinder interior volume. Figure 1 shows a diagram of the problem geometry and the fluid domain.

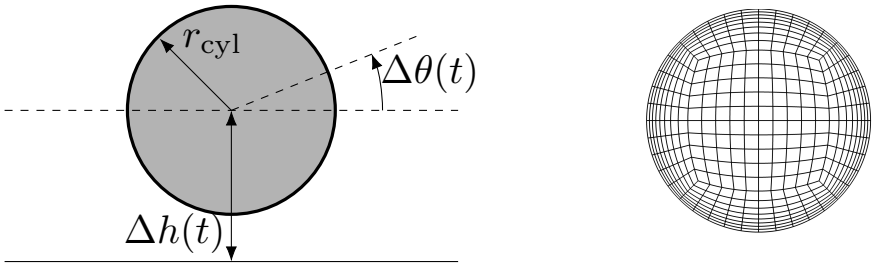

(a) Geometry diagram. **(b) Fluid domain.**

Figure 1: Cylinder problem description.

B. Motion

Four prescribed motions are defined for this problem. They are designed to target the properties of translation (Motion 1), rotation (Motion 2), deformation (Motion 3), and a composite (Motion 4) as presented in Figure 2. The motion descriptions for translation ($\Delta h(t)$), rotation ($\Delta\theta(t)$), deformation ($x(x_0,t), y(y_0,t)$), and the composite are given in Table 1. Relevant constants for all motions are listed in Table 2. All cases shall be run from $t = 0$ until $t = 2$ for a total duration of 2 time units. A_θ is a rotation amplitude (Motion 2), A_a is an amplification factor for the deformation of a circle into an ellipse (Motion 3), and r_{cyl} is the initial radius of the cylinder wall for all motions. The prescribed-motion function for Motions 1 & 2 is

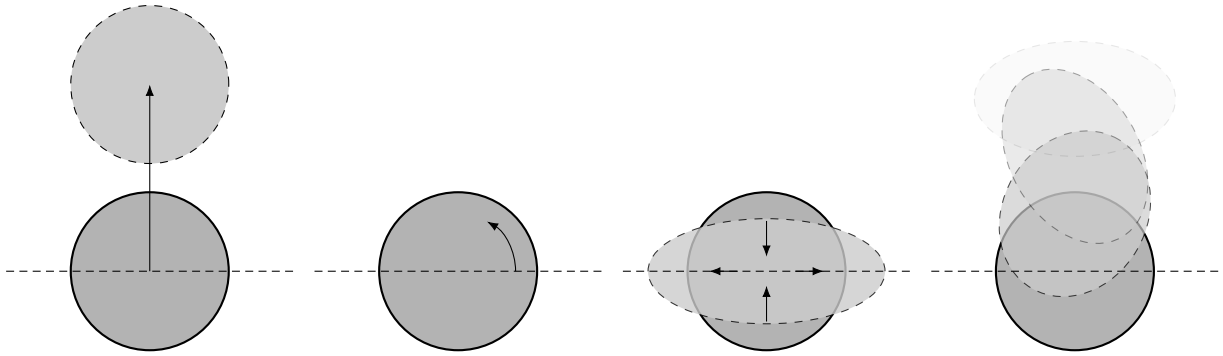

(a) Motion 1: Translation **(b) Motion 2: Rotation** **(c) Motion 3: Deform** **(d) Motion 4: Composite**

Figure 2: Cylinder motion descriptions.

	Motion 1	Motion 2	Motion 3	Motion 4
$\Delta h(t)$	$\alpha(t)$	0	–	–
$\Delta\theta(t)$	0	$A_\theta \cdot \alpha(t)$	–	–
$x(x_0, t)$	–	–	$x_0 \cdot \psi(t)$	Eq. 3
$y(y_0, t)$	–	–	$y_0 \,/\, \psi(t)$	Eq. 3

Table 1: Cylinder prescribed-motion test cases, $t \in [0, 2]$

r_{cyl}	0.5
A_θ	π
A_a	1.5

Table 2: Cylinder motion constants.

defined as

$$\alpha(t) = t^3 \left(8 - 3t\right) / 16$$

which varies from 0 to 1 on the interval $t = [0, 2]$. The prescribed-motion for Motion 3 is of a cylinder deforming into an ellipse such that the interior area remains constant during deformation. The deformation function is given as

$$\psi(t) = 1 + (A_a - 1)\alpha(t) \tag{1}$$

1. Motion 4: Composite

The fourth motion is defined as a composite of the three primitive motions; including translation, rotation, and deformation. The intent of this case in the test suite is to break any intrinsic symmetries in the flow field that may cause symmetric error contributions to cancel each other out; causing certain implementation errors to pass a test undetected. The composite motion is formed by representing the primitive motions as transformation matrices and composing them by matrix multiplication. Note, translation is not a linear transformation in (x, y)-space. However, translation can be accommodated by augmenting the transformation to $(x, y, 1)$-space. The composite transformation is formulated as

$$\begin{bmatrix} x \\ y \\ 1 \end{bmatrix} = \begin{bmatrix} 1 & 0 & 0 \\ 0 & 1 & \alpha(t) \\ 0 & 0 & 1 \end{bmatrix} \begin{bmatrix} \cos(A_\theta \alpha(t)) & -\sin(A_\theta \alpha(t)) & 0 \\ \sin(A_\theta \alpha(t)) & \cos(A_\theta \alpha(t)) & 0 \\ 0 & 0 & 1 \end{bmatrix} \begin{bmatrix} \psi(t) & 0 & 0 \\ 0 & \frac{1}{\psi(t)} & 0 \\ 0 & 0 & 1 \end{bmatrix} \begin{bmatrix} x_0 \\ y_0 \\ 1 \end{bmatrix} \tag{2}$$

Expanding the transformations yields the following explicit form of the composite motion

$$\begin{aligned} x(x_0, y_0, t) &= \left[\psi(t) x_0 \cos(A_\theta \alpha(t)) - \frac{1}{\psi(t)} y_0 \sin(A_\theta \alpha(t))\right] \\ y(x_0, y_0, t) &= \left[\psi(t) x_0 \sin(A_\theta \alpha(t)) + \frac{1}{\psi(t)} y_0 \cos(A_\theta \alpha(t))\right] + \alpha(t) \end{aligned} \tag{3}$$

which is differentiated with respect to time yielding the velocity components

$$\begin{aligned} v_x(x_0, y_0, t) = &\left[\frac{d\psi}{dt} x_0 \cos(A_\theta \alpha(t)) - \psi(t) x_0 A_\theta \frac{d\alpha}{dt} \sin(A_\theta \alpha(t))\right] - \ldots \\ &\left[-\frac{d\psi}{dt} \frac{1}{\psi(t)^2} y_0 \sin(A_\theta \alpha(t)) + \frac{1}{\psi(t)} y_0 A_\theta \frac{d\alpha}{dt} \cos(A_\theta \alpha(t))\right] \\ v_y(x_0, y_0, t) = &\left[\frac{d\psi}{dt} x_0 \sin(A_\theta \alpha(t)) + \psi(t) x_0 A_\theta \frac{d\alpha}{dt} \cos(A_\theta \alpha(t))\right] + \ldots \\ &\left[-\frac{d\psi}{dt} \frac{1}{\psi(t)^2} y_0 \cos(A_\theta \alpha(t)) - \frac{1}{\psi(t)} y_0 A_\theta \frac{d\alpha}{dt} \sin(A_\theta \alpha(t))\right] + \frac{d\alpha}{dt} \end{aligned} \tag{4}$$

C. Governing equations and flow conditions

The governing equations for this problem are 2D compressible Euler and Navier-Stokes with a constant ratio of specific heats equal to 1.4 and a Prandtl number of 0.72. For the Euler calculations, the cylinder interior is prescribed to have no normal velocity on the wall. For viscous calculations, the cylinder interior is prescribed with a no-slip, adiabatic wall boundary condition. The initial condition at time $t = 0$ is given by the conserved-variable state vector

$$\boldsymbol{u}|_{t_0} = [\rho, \rho v_1, \rho v_2, \rho E]|_{t_0} = [1, 0, 0, 50.]$$

For each test case, a range of Reynolds numbers should be simulated. The reference velocity is chosen to be 1.0 and the reference length scale is the cylinder diameter, $d = 2r_{\text{cyl}} = 1.0$. Three Reynolds numbers are considered for the cylinder: $Re = \infty$ (Euler), $Re = 1000$, and $Re = 10$.

D. Preliminary results

Some preliminary results for the cylinder test case have been produced and a subset for the $Re = 10$ flow condition is included here to give insight into expected solution and output behaviors. Figure 3 shows contours of x-momentum for all motions at $Re = 10$, which exhibit a variety of modal dynamics that are excited from the cylinder motion. Force and work histories are shown in Figure 4. Time-history comparisons show good agreement between results from the Air Force Research Laboratory and University of Michigan. For Motion 1, there is generally good agreement between all data sets, but there are some small yet significant discrepancies in the time histories. That such discrepancies are observed is a positive outcome for the cylinder test case since it provides a simpler platform to try and identify the source of observed differences. Finally, a rigorous study of output convergence was conducted at the University of Michigan, and these results are included in Appendix A.

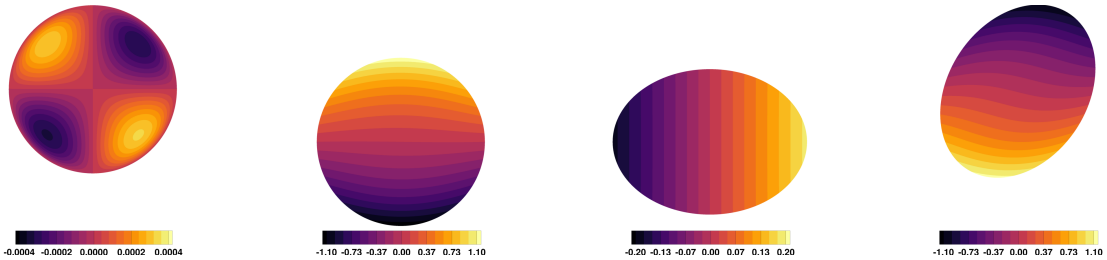

(a) Motion 1 **(b) Motion 2** **(c) Motion 3** **(d) Motion 4**

Figure 3: Cylinder contours of x-momentum for motions at time $t = 1.5$ and Reynolds number $Re = 10$.

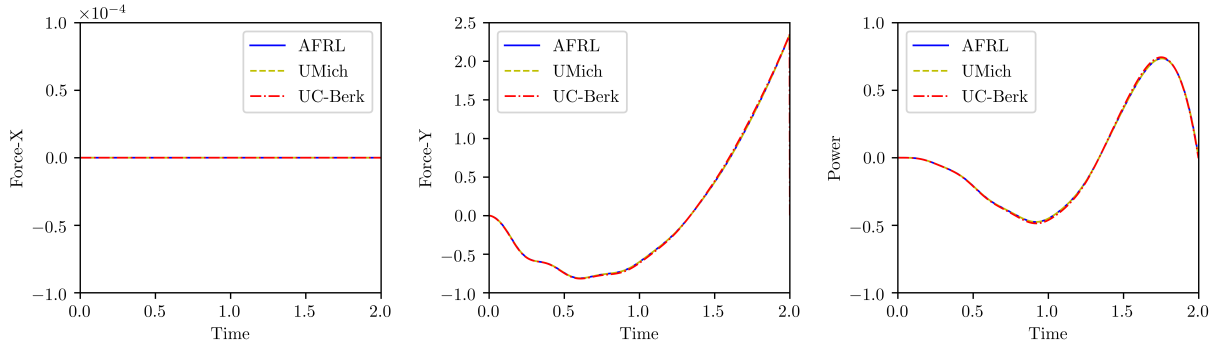

(a) Motion 1 (translation), $Re = 10$

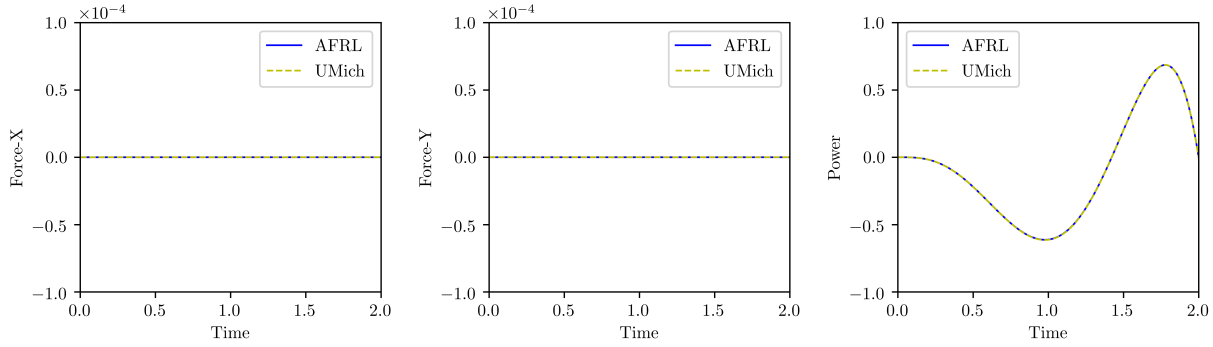

(b) Motion 2 (rotation), $Re = 10$

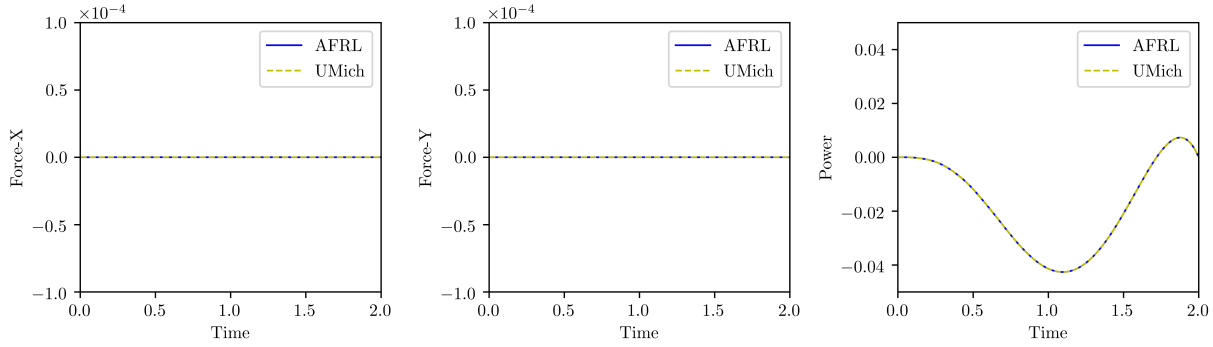

(c) Motion 3 (deformation), $Re = 10$

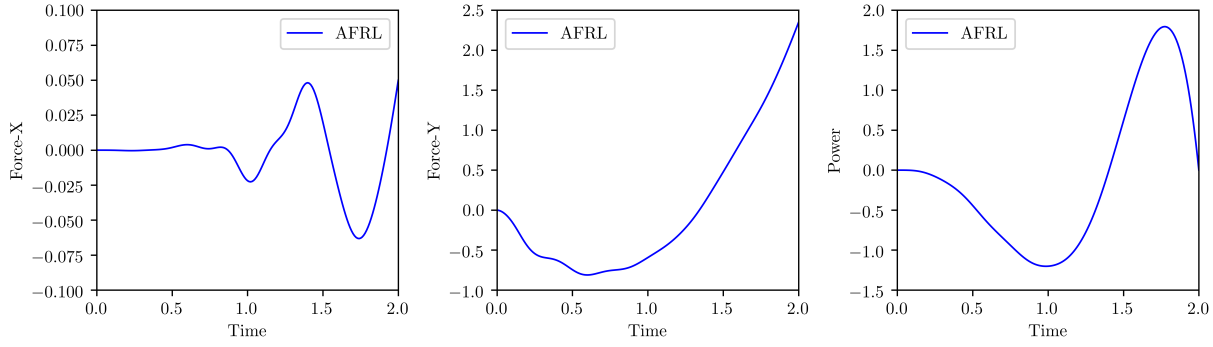

(d) Motion 4 (composite), $Re = 10$

Figure 4: Force and power histories for cylinder test cases at $Re = 10$**.**

III. Heaving-pitching airfoil

These cases involve a NACA 0012 airfoil undergoing a smooth flapping-type motion, starting from rest at zero angle of attack and ending at a one chord length higher position at the end of the motion at time T. Two motions are considered at one Reynolds number, Re = 1000, based on the chord length.

A. Geometry

The geometry consists of a NACA 0012 airfoil with chord length $c = 1$, with geometry modified to give zero trailing edge thickness:

$$y(x) = \pm 0.6(0.2969\sqrt{x} - 0.1260x - 0.3516x^2 + 0.2843x^3 - 0.1036x^4), \quad x \in [0, 1].$$

The far-field boundary should be located at least 100 chord-lengths away from the airfoil.

B. Motion

The airfoil undergoes a smooth upward motion of one chord length for the duration of $T = 2$ time units, by heaving and pitching about a point located at the airfoil 1/3 chord location (see figure). We consider two different motions with different properties. In addition to the prescribed motion function defined for the cylinder test case, we define one additional function here:

$$\beta(t) = -t^6 + 6t^5 - 12t^4 + 8t^3$$

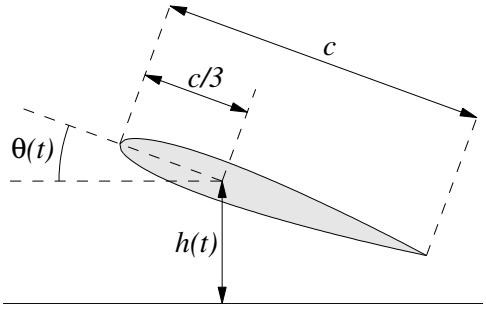

Table 3 presents the two motion descriptions in terms of vertical and angular displacements, where $\alpha(t)$ is the same prescribed motion function used for the cylinder test case and $B_\theta = 80\pi/180$.

	Motion 1	Motion 2
$\Delta h(t)$	$\alpha(t)$	$\alpha(t)$
$\Delta\theta(t)$	0	$B_\theta \cdot \beta(t)$

Table 3: Heaving-pitching airfoil prescribed-motion test cases, $t \in [0, 2]$

Note, the general heaving-pitching airfoil test case has been used in previous workshops. However, the motions defined in this document differ from those that have been used in previous workshops. In particular, the motions defined in the present work have been modified with higher levels of smoothness in the prescribed motion functions. Due to the change in prescribed motions, results and conclusions from previous studies may not be comparable to the present test case.

C. Governing equations and flow conditions

The governing equations for this problem are the 2D compressible Navier-Stokes equations with a constant ratio of specific heats equal to 1.4 and a Prandtl number of 0.72. Two boundary conditions are imposed: far-field characteristic conditions at the outer domain and no-slip adiabatic wall condition on the moving airfoil.

The free-stream has a Mach number $M_\infty = 0.2$ and is horizontal. The Reynolds number based on the chord of the airfoil is Re = 1000. The initial condition at time $t = 0$ is the steady-state solution for the initial position $h = 0$, $\theta = 0$. To simplify post-processing, we assume convenient units in which the airfoil chord is $c = 1$ and the free-stream density and speed are unity, so that the free-stream conservative state vector is

$$[\rho, \rho u, \rho v, \rho E] = \left[1,\ 1,\ 0,\ 0.5{+}1/[M^2\gamma(\gamma - 1)]\right]$$

D. Preliminary results

A subset of results are presented here to give insight into the behavior for the heaving-pitching airfoil problem. Figure 5 shows contours of vorticity for both prescribed motions, where a variety of vortical flow structures are present in the flow field. Additionally, Figure 6 shows time-histories for output quantities for each motion.

(a) Motion 1: Heaving @ $t = 1.5$ **(b) Motion 2: Heaving + Pitching @ $t = 0.5$**

Figure 5: Heaving-pitching airfoil contours of vorticity for motions at intermediate-time.

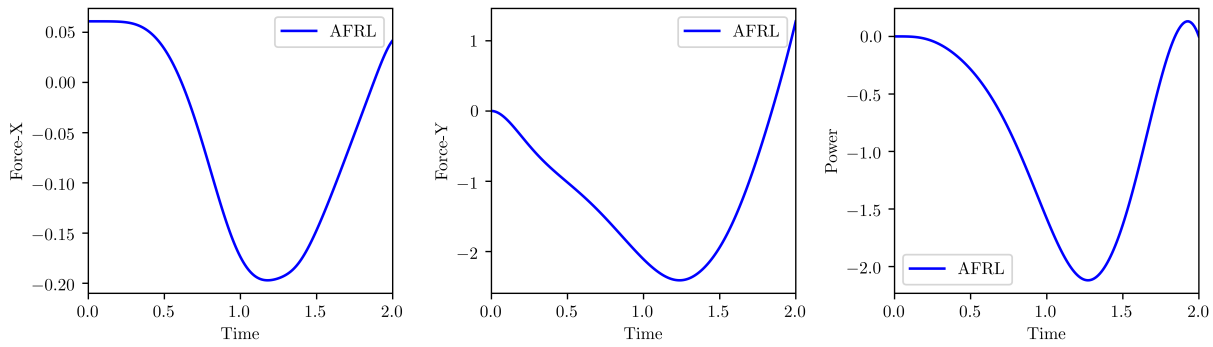

(a) Motion 1 (translation)

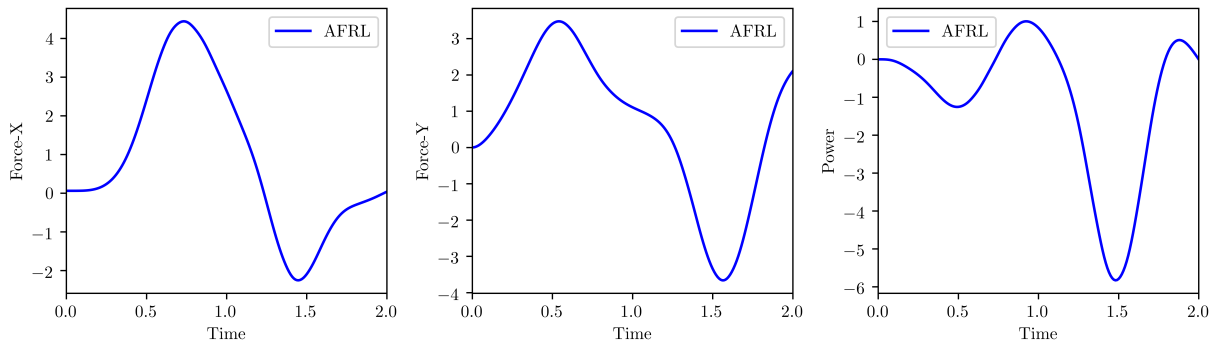

(b) Motion 2 (translation + rotation)

Figure 6: Force and power histories for airfoil test cases.

IV. Outputs

A. Work

The requested output quantities are defined similarly for both the cylinder and the airfoil cases. The first output is the work (energy) that the fluid exerts on the surface of the cylinder/airfoil during the motion,

which can be written as

$$W = \int_0^T \vec{F}(t) \cdot \vec{v}_0 dt + \int_0^T \vec{\tau}(t) \cdot \vec{\omega}_0 dt = \int_0^T F_y(t)\dot{h}(t)dt + \int_0^T \tau_z(t)\dot{\theta}(t)dt \tag{5}$$

Here, $\vec{F}(t) = [F_x(t), F_y(t)]$ is the force imparted by the fluid on the surface, $\vec{\tau}(t) = [0, 0, \tau_z(t)]$ is the torque imparted by the fluid on the surface about the reference pivot point (cylinder center, airfoil 1/3 chord), $\vec{v}_0 = \dot{h}(t)$ is the velocity of the pivot point, and $\vec{\omega}_0 = [0, 0, \dot{\theta}]$ is the angular velocity of the cylinder/airfoil about the pivot point. Note, that this output can be equivalently computed as

$$W = \int_0^T \int_{\text{surface}} \vec{v}_G(t) \cdot \vec{f}_{\text{surf}}(t)\, ds\, dt \tag{6}$$

where $\vec{v}_G(t)$ is the velocity of the surface and $\vec{f}_{\text{surf}}(t)$ is the surface stress vector.

B. Impulse

The second output is the vertical impulse from the fluid onto the surface during the motion,

$$I = \int_0^T F_y(t)dt \tag{7}$$

C. Mass conservation

For the *Flow In A Cylinder* test case, the fluid mass should remain constant for all time. The error in mass conservation accumulated over time shall be computed as

$$e_m = \frac{1}{T} \int_0^T (m_t - m_0)^2\, dt \tag{8}$$

where m_0 is the initial fluid mass integrated discretely at time $t = 0$ and m_t is the fluid mass integrated discretely at a given time t. The fluid mass shall be computed as

$$m_t = \int_{\text{volume}} \rho(t)dV \tag{9}$$

V. Requirements

The requirements for full participation in this test suite are as follows:

1. Perform the indicated simulation for the test cases. Calculate the quantities W and I for each case, and perform a grid/timestep convergence study to get the values as accurate as possible. Record the work units (WU) [1].

2. Provide the work units, the converged output values, nDOFs in the discretization (spatial and temporal), and the distance to the far-field boundary (aifoil case) for each simulation. Submit this data to the case organizers, using the template shown below.

3. Describe in detail the mesh-motion formulation that was used to generate the results. This includes motion implementation, transformation equations, boundary treatment, and any underlying assumptions.

Partial data for a subset of test cases will also be accepted for making meaningful comparisons.

VI. Summary

This is an invited paper for the SciTech 2021 special session: High-Fidelity CFD Preworkshop. It describes cases for the Mesh Motion test suite, which will be part of the workshop test cases. The objective

Geometry	Motion	Re	W	I	e_m	space nDOF	time nDOF	Work Units
Cylinder	1	∞	-	-	-	-	-	-
⋮								
Airfoil	1	1000	-	-	N/A	-	-	-
⋮								

Table 4: Template for team contributions. The spatial nDOF does not include the equation state rank. The temporal nDOF is the number of time steps times the number of stages per time step (in a multistage time integration).

of including this suite in the workshop is to identify implementation differences and common errors in high-fidelity simulations on deforming domains. Such simulations are increasingly of interest in applications such as aeroelasticity and other fluid-structure interaction problems. As previous workshops have identified persistent discrepancies in the results of the participants, the focus on the present suite of problems is simplicity and smoothness. To this end, two problems have been constructed for the purpose of verifying and quantifying the performance and accuracy of high-order fluids solvers: one involving internal flow and the deformation of a cylinder, and another involving external flow around a moving airfoil. In both cases, the temporal variations have been constructed with increased high-order differentiability at the initial time, to prevent startup transients and hence to aid in temporal convergence studies.

Geometry descriptions, prescribed motions, and deformations have all been defined for these problems and documented in this paper along with preliminary results as a reference for workshop participants. Output quantities of interest have been identified and data reporting requirements and format have been laid out to facilitate data assembly from workshop participants. The case organizers encourage wide participation from multiple groups, even with partial data for some of the cases, to help in drawing meaningful conclusions and recommendations.

References

[1] Wang, Z., Fidkowski, K., Abgrall, R., Bassi, F., Caraeni, D., Cary, A., Deconinck, H., Hartmann, R., Hillewaert, K., Huynh, H., Kroll, N., May, G., Persson, P.-O., van Leer, B., and Visbal, M., "High-Order CFD Methods: Current Status and Perspective," *International Journal for Numerical Methods in Fluids*, 2013. doi:10.1002/fld.3767.

[2] Fidkowski, K. J., "Output-Based Space-Time Mesh Optimization for Unsteady Flows Using Continuous-in-Time Adjoints," *Journal of Computational Physics*, Vol. 341, No. 15, 2017, pp. 258–277. doi:10.1016/j.jcp.2017.04.005.

VII. Appendix A: Convergence Studies

Space and time convergence studies were performed for the cylinder test cases, using the first three motions and all three Reynolds numbers. Both triangular and quadrilateral meshes were studied, but for conciseness only the quadrilateral mesh results are presented here. In time, the ESDIRK-5 method was used with 256 uniform time steps. A temporal convergence study was also performed, and this showed that temporal errors dominated the spatial errors when the temporal resolution was not this high, particularly for the finer meshes and higher spatial orders. Presently, only the spatial convergence of the outputs is shown.

Three meshes were used at each order, and these are shown in Figure 7. The elements on the perimeter of the cylinder are curved to $q = 4$ geometry approximation. Note that only a single layer of elements is curved, so that the boundary quadrilaterals have one edge curved and the other edges straight.

The impulse and work output convergence histories are shown in Figures 8 and 9. These plots show the output values (linear scale) versus the spatial degrees of freedom (log scale), for spatial orders $p = 1 - 4$. The outputs were measured by a spatial integration along the cylinder perimeter, and a temporal integration over the given time horizon. The time integration for ESDIRK5 was performed by three-point quadrature in each time step, using state values reconstructed as cubic functions from the two adjacent time nodes [2]

Many of the impulse outputs approach zero, as expected by symmetry, and hence the results for these

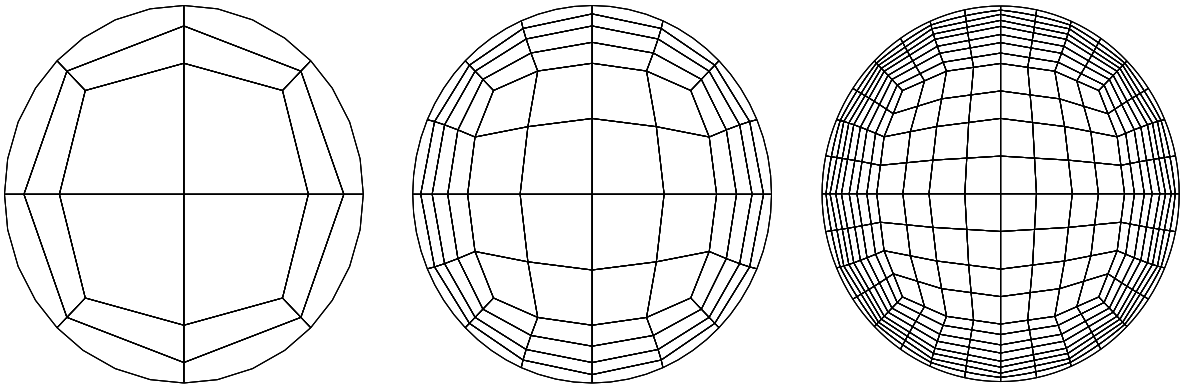

(a) Mesh 0 **(b) Mesh 1** **(c) Mesh 2**

Figure 7: Cylinder output convergence studies: meshes

convergence studies are not overly meaningful. For nonzero output values, particularly in the work, we see that the outputs appear to converge as the number of degrees of freedom (mesh size/order) is increased.

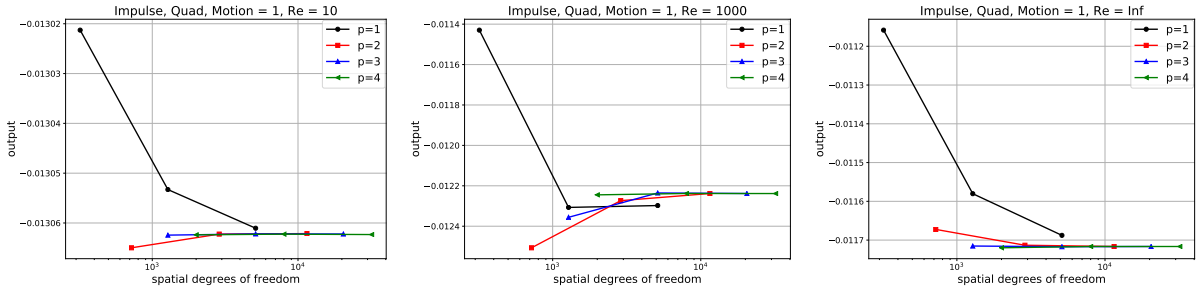

(a) Motion 1 (translation).

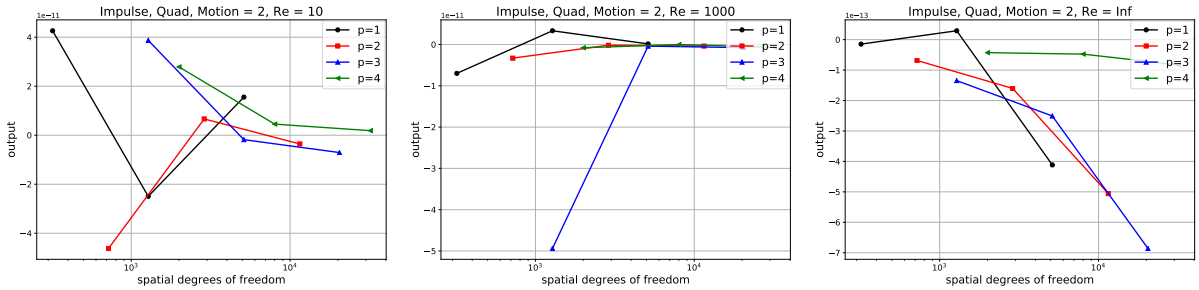

(b) Motion 2 (rotation).

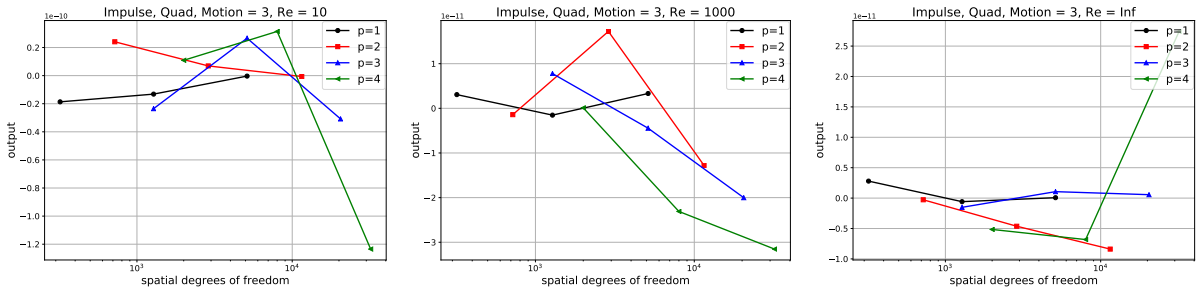

(c) Motion 3 (deformation).

Figure 8: Cylinder output convergence studies: Impulse

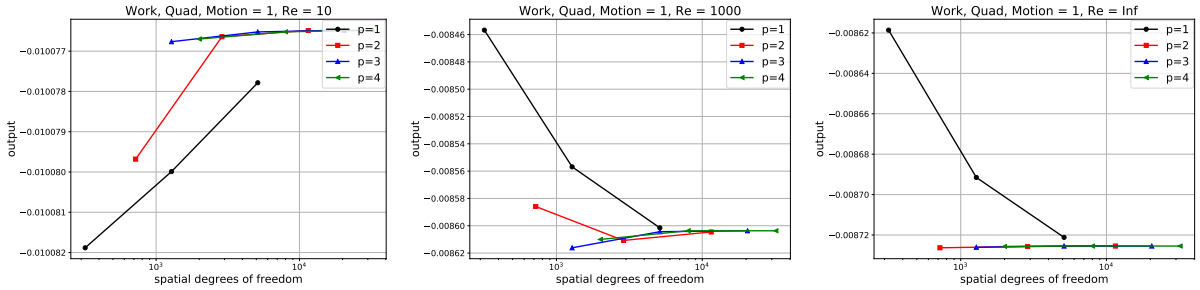

(a) Motion 1 (translation).

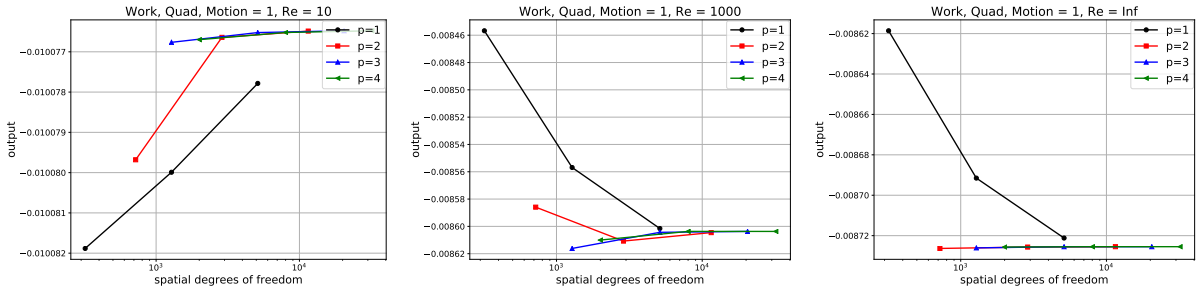

(b) Motion 2 (rotation).

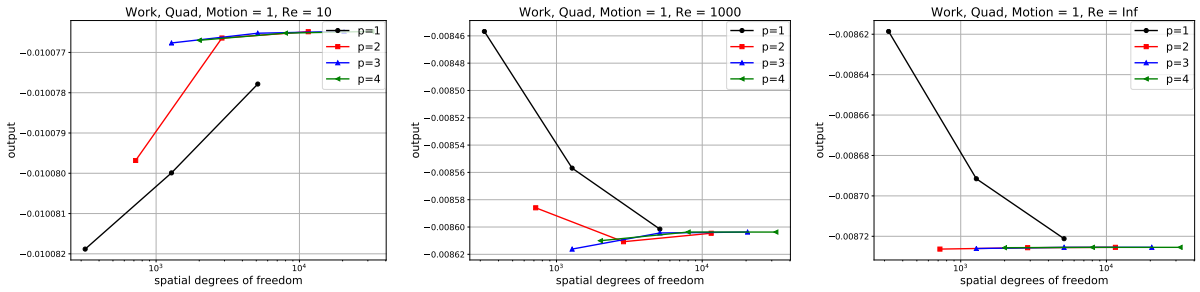

(c) Motion 3 (deformation).

Figure 9: Cylinder output convergence studies: Work